Materials Sciences and Applications, **2011, 2, 1584-1592**
doi:10.4236/msa.2011.211212 Published Online November 2011 (http://www.SciRP.org/journal/msa)

Solid State Reactions in Cr_2O_3-ZnO Nanoparticles Synthesized by Triethanolamine Chemical Precipitation

Imelda Esparza[1,2], Myriam Paredes[1], Roberto Martinez[2], Adriana Gaona-Couto[1], Guadalupe Sanchez-Loredo[1], Luisa M. Flores-Velez[3], Octavio Dominguez[1*]

[1]Instituto de Metalurgia-UASLP, Sierra Leona, México; [2]CIMAV, Cervantes, México; [3]Facultad de Ciencias Químicas-UASLP, Sierra Leona, México.
Email: *nanochemmex@yahoo.com

Received August 27th, 2011; revised October 1st, 2011; accepted October 16th, 2011.

ABSTRACT

The present work reports the preliminary results about solid state reactions of Cr-ZnO solid solutions and $ZnCr_2O_4$ nanometric particles obtained with triethanolamine (TEA). Different compositions were prepared from 0.65 to 33.3 at% chromium, the last one corresponding to $ZnCr_2O_4$ cubic spinel composition. Fourier Transform Infrared Spectroscopy (FTIR) together with X-ray diffraction (XRD) patterns of powders with Cr^{3+} between 0.65 and 16.0 at% were assigned to Cr-ZnO solid solution due to the only presence of ZnO structure, FTIR spectra indicating that Cr-O bonding exists even if there was no presence of $ZnCr_2O_4$. With low chromium atomic percent, lattice parameters increase, but as the chromium content exceeds of 3 at%, there is basically no further expansion of the cell. From Williamson-Hall and Rietveld methods the lattice dimensions were assigned to chromium incorporation in ZnO structure and the lattice contraction by particle size refinement. After annealing all samples from 0.65 to 16.0 at% at 400˚C in oxygen, the analysis showed that nanoparticles of Cr-ZnO solid solution still remain.

Keywords*: *Nanometric $ZrCr_2O_4$ Spinel*, *Cr-ZnO Nanoparticles*, *Thermal Analysis*, *FTIR*, *Chemical Preparation

1. Introduction

Chromium (III) oxide has a wide range of applications including pigments to reflect infrared radiation [1], heterogeneous catalysts [2], coating materials for thermal protection, wear resistance [3], and so on. It has been established that some spinels have advanced gas sensing and catalytic properties [4], so $ZnCr_2O_4$ could be a suitable sensors for aggressive environments because chromium improves the stability of ZnO films against diluted hydrochloric and nitric acid media [5]. Besides Cr_2O_3-ZnO materials, specially prepared in nanocrystalline state are interesting systems for H_2 production via photoelectrochemical splitting of water [6].

A number of synthetic routes have been employed to synthesize ZnO-Cr_2O_3 nanoparticles such as chemical vapor synthesis (CVS) [7], ball milling [8], spray pyrolysis [9], decomposition of coprecipitated hydroxides [10] and calcinations of metallo-organic precursor solutions [11]. Because triethanolamine is extensively used in industrial milling to avoid agglomeration and in cosmetic and food products as dispersant agent, its present price is low and quite competitive. Therefore, the present work reports the preliminary results about a novel, technically simple and more economical process for producing $ZnCr_2O_4$ and high chromium-ZnO solid solution nanometric particles.

2. Experimental Procedure

Chromium (III) nitrate nonahydrate ($Cr(NO_3)_3 \cdot 9H_2O$, Sigma-Aldrich 99%) and zinc (II) nitrate hexahydrate ($Zn(NO_3)_2 \cdot 6H_2O$, Sigma-Aldrich 99%) were used as the chromium and zinc ions sources respectively, and triethanolamine $N(CH_2CH_2OH)_3$ (TEA, Sigma-Aldrich 98%) was used as the base in a variation of the procedure reported before for ZnO precipitation [12]. All experiments were carried out by simultaneous addition at 25 mL/s of each metal ion solution, Zn^{2+}(aq) and Cr^{3+}(aq) at different concentrations, simultaneously with the TEA solution to a third water solution, all heated at 80˚C and then mixed for 15 minutes at pH ≈ 9. After filtering, the

samples were washed several times with acetone to remove TEA. When the concentration of Cr^{3+} reaches the stoichiometric cationic ratio of Zn:Cr = 1:2, $ZnCr_2O_4$ spinel becomes the final product.

3. Instrumental Techniques

Crystal structure and phase composition of the samples were determined by X-ray diffraction using a Rigaku DMAX-1000 diffractometer with Cu K_α (λ = 1.54056 Å) radiation. The XRD data was collected in the range 10 < 2θ < 80˚ with a step size of 0.01˚ and an integration time of 2 seconds. Fourier Transform Infrared Spectroscopy (FTIR) of the samples was carried out using a Perkin-Elmer SPECTRUM-GX spectrophotometer scanning between 3000 and 400 cm^{-1}. Samples were prepared by mixing about 2% of synthesized powder with KBr. The TEM specimens were prepared by dispersing the powder in n-hexane with the aid of ultrasonic agitation. Drops were poured into a carbon supported copper grid, and then dried in air. The TEM images were obtained using a JEOL 1200 transmission electron microscope having an EDS spectrometer and operated at an acceleration voltage of 120 kV. Thermal analysis was performed using a Perkin-Elmer DTA7 differential thermal analyzer. The instrument was operated using chromatographic O_2 (Praxair, 99.999%) and a constant heating rate of 10˚C /min.

4. Results and Discussion

4.1. As-Prepared Zinc Oxide and Chromium Oxide

The aqueous reaction between Zn^{2+} and TEA always produced ZnO samples presenting the wurtzite structure (hexagonal phase, space group $P6_3mc$). The XRD patterns of the as-prepared nanometric ZnO were compared with a standard and are shown in **Figure 1(a)**, all the diffraction peaks being well assigned to hexagonal phase ZnO as reported in JCPDS card No. 36-1451. The representative TEM image of the as-prepared ZnO nanoparticles is shown in **Figure 1(b)**, indicating that particles present spherical-like morphology and narrow size distribution, having a particle size between 30 and 50 nm. The IR spectra of nanometric ZnO is exhibited in **Figure 1(c)**. It shows the presence of several absorption bands indicating a minor shift from those reported in the literature, 1633, 1555, 1384, 970, 833, 679 and 566 cm^{-1} [13].

On the other hand, Cr_2O_3 (rhombohedral phase, space group $R\bar{3}c$) was obtained from the aqueous reaction between Cr^{3+} and TEA solutions. After being washed and filtrated, the powder was calcinated in electric oven at 400˚C to crystallize the chromium oxide.

The XRD pattern of the nanometric Cr_2O_3 is shown in

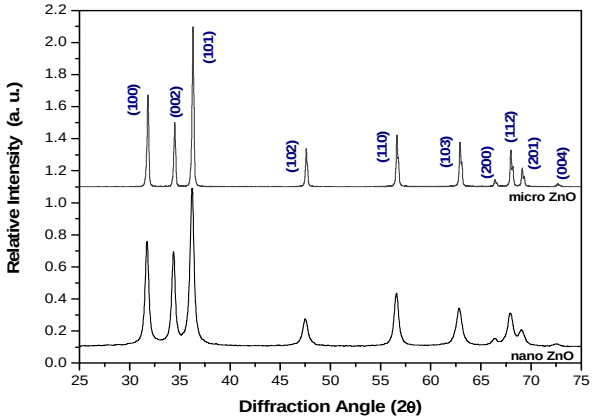

(a)

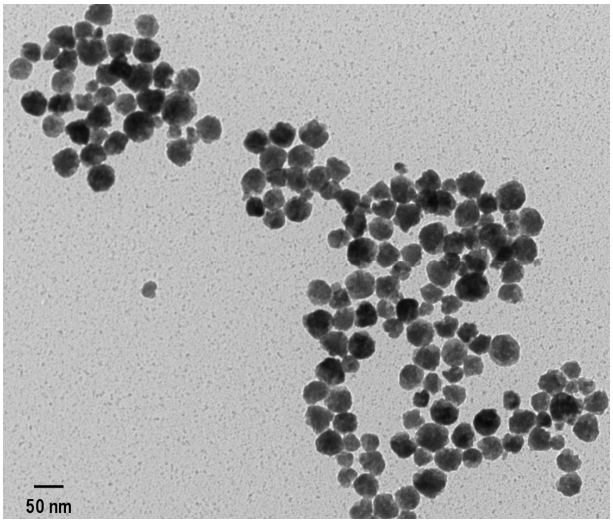

(b)

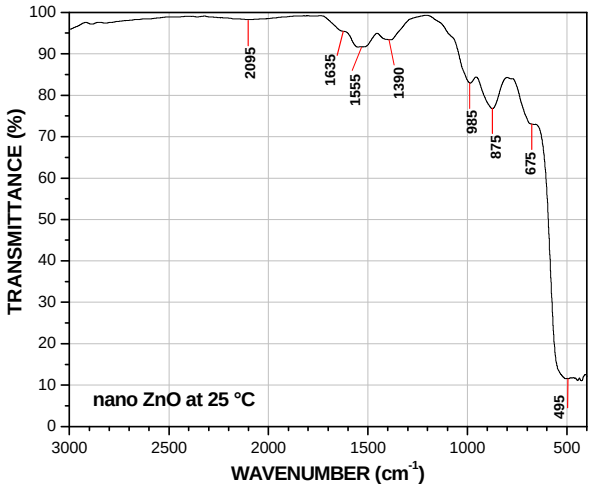

(c)

Figure 1. (a) X-ray diffraction pattern of micrometric ZnO and as-prepared zinc oxide nanoparticles; (b) TEM image of the as-prepared nanometric zinc oxide particles; (c) FTIR of the nanometric ZnO.

Figure 2(a), all diffraction peaks being assigned to JCPDS card No. 38-1479. The representative TEM image of the obtained Cr_2O_3 is shown in **Figure 2(b)** and the corresponding IR spectra is shown in **Figure 2(c)**.

The TEM image of the prepared Cr_2O_3 nanoparticles indicated that particles present rhomboidal-like morphology and particle size between 25 and 50 nm. The IR spectra of nanometric Cr_2O_3 (**Figure 2(c)**) shows the presence of some absorption bands reported in the literature (1633, 1505, 1024, 910, 800, 615 and 545 cm^{-1}) [14].

4.2. Prepared Zinc-Chromium Oxide Nanoparticles

Precipitation products from the reaction between Zn^{2+} and Cr^{3+} ions with TEA were obtained incorporating different amounts of the chromium salt. The obtained zinc-chromium oxide powders were analyzed by XRD technique following Rietveld procedure using the MAUD software [15] and some of their corresponding patterns are shown in **Figure 3**. In these cases, the particle size and the lattice strain contribution to the X-ray diffraction peak broadening was estimated using Williamson-Hall analysis [16]. Assuming that the particle size and strain contributions to line broadening are independent from each other and both have a Cauchy-like profile, the observed line breadth is simply the sum of the two contributions leading to the Williamson-Hall equation [16]:

$$\beta_{hkl}\cos\theta_{hkl} = (K\lambda/L) + \eta\sin\theta_{hkl} \qquad (1)$$

β_{hkl} corresponding to broadening and $\eta = 4\varepsilon$, ε being the root mean square value of microstrain. Plotting the value of $\beta_{hkl}\cos\theta_{hkl}$ as a function of $\sin\theta_{hkl}$ the microstrain may be estimated from the slope of the line and the particle size ***L*** from the intersection with the vertical axis.

Aqueous reaction experiments using different zinc-chromium concentrations up to the stoichiometric ratio $[Cr^{3+}] = 2[Zn^{2+}]$ were performed using the same conditions as described before. The obtained zinc-chromium oxides were analyzed by XRD. **Figure 3(a)** shows the corresponding XRD patterns where diffraction peaks were completely assigned to the presence of ZnO for those concentrations up to 16.0 at% of Cr^{3+}. At a chromium content of 16 at%, there is no more Cr_2O_3-ZnO solid solution and some other Cr_xZn_yO compound precipitates; at present there is no crystal structure linked to such compound, but diffraction peaks could be assigned to JCPDS card No. 11-0277 associated to amorphous $2ZnO{\cdot}Cr_2O_3{\cdot}H_2O$. When the spinel composition was reached (33.3 at%), the new phase was evident by the presence of peaks corresponding to the $ZnCr_2O_4$ cubic structure with a space group $Fd\bar{3}m$, all diffraction peaks being assigned to $ZnCr_2O_4$ as reported in JCPDS

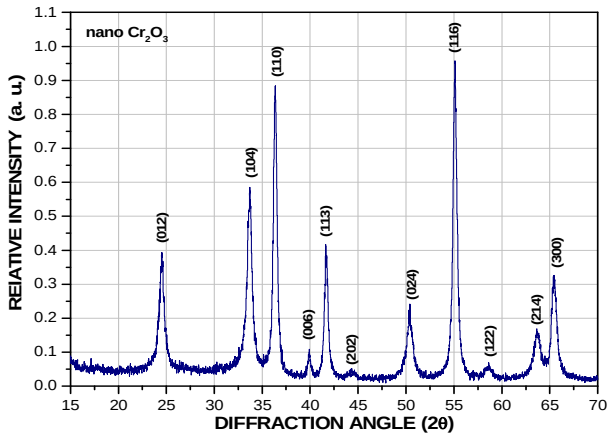

(a)

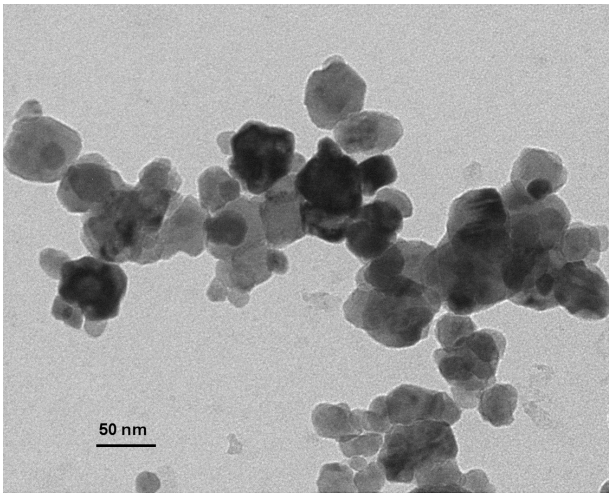

(b)

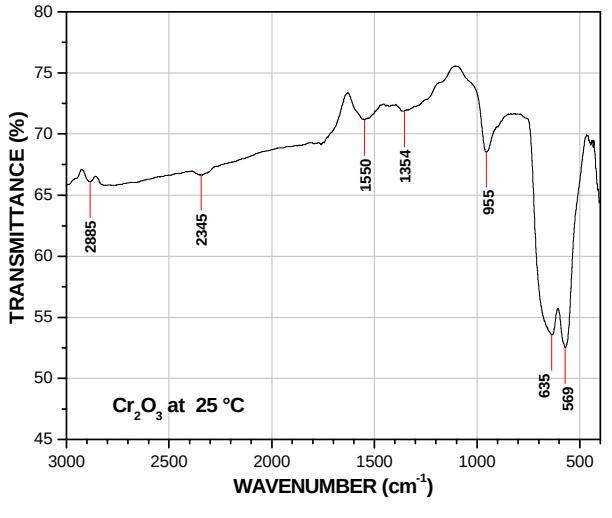

(c)

Figure 2. (a) X-ray diffraction pattern of prepared chromium oxide nanoparticles; (b) TEM bright field image and (c) FTIR spectra of the nanometric Cr_2O_3 particles.

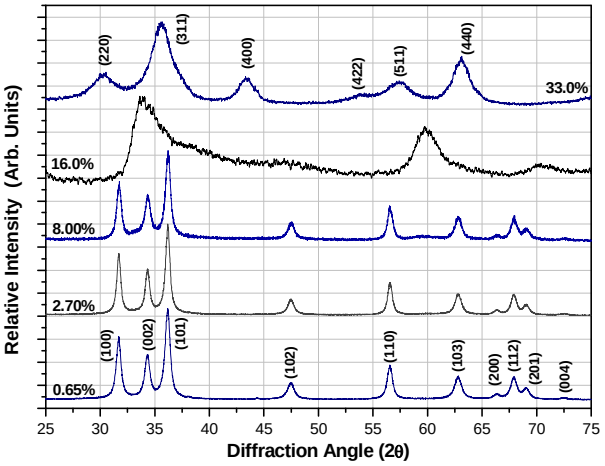

(a)

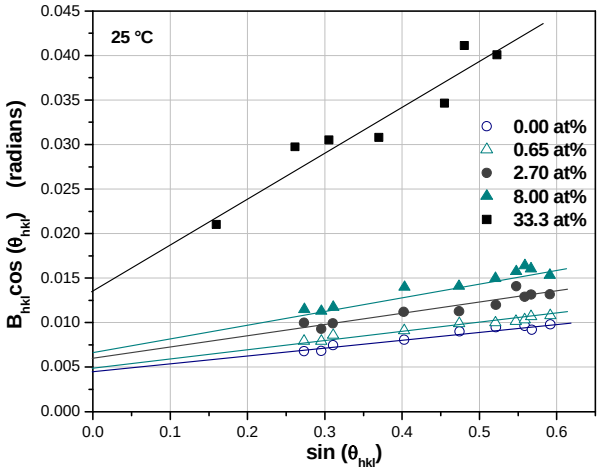

(b)

Figure 3. (a) XRD pattern and (b) Williamson-Hall plots of the different nanometric ZnO/xCr_2O_3 particles.

card No. 22-1107. Because line broadening was important, Rietveld and Williamson-Hall analysis were used to get information about lattice parameter, strain distortion and particle size in samples as a function of the chromium content. **Figure 3(b)** shows the Williamson-Hall plots obtained after using equation (1) on XRD data from each sample at room temperature. According to the calculated slope η and intersection with vertical axis (λ/L) from **Figure 3(b)**, slope augmented and particle size was slightly reduced as Cr^{3+} was incorporated in the ZnO structure (**Table 1**). Once the spinel composition was reached, the particle refinement was notorious. Moreover, Rietveld analysis was performed to each Cr-ZnO solid solution to find the lattice parameters ***c*** and ***a*** (**Table 1**) of the hexagonal ZnO structure. TEM bright field image is shown on **Figure 4(a)** to illustrate a mean particle size of 25 nm, corroborating the particle size calculated from Williamson-Hall method. **Figure 4(b)** corresponds to the Rietveld refinement of the same sample, proving that the

Table 1. Chemical Composition, Particle size (L), Lattice Distortion (η) and Lattice Parameters (*a* and *c*) Obtained from Nanometric ZnO-Cr_2O_3 Powders.

Chromium (at%)		Williamson-Hall Analysis		Rietveld Analysis	
Nominal	**EDS**	**<L> (nm)**	**η (%)**	***a* (Å)**	***c* (Å)**
0.00	0.00	45	0.87	3.2466	5.2044
0.65	0.50	33	0.88	3.2489	5.2100
2.70	2.49	25	1.22	3.2509	5.2094
8.00	7.86	22	1.85	3.2515	5.2117
16.0	15.40	15*	------	--------	--------
33.3	34.16	11	4.98	8.3327	--------

*Estimated from TEM images.

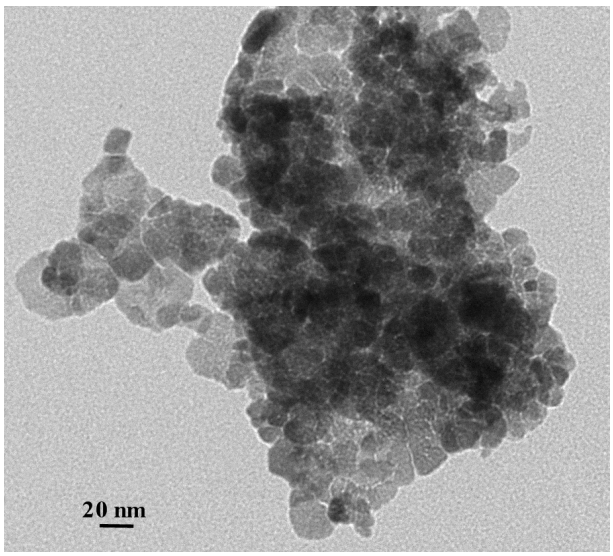

(a)

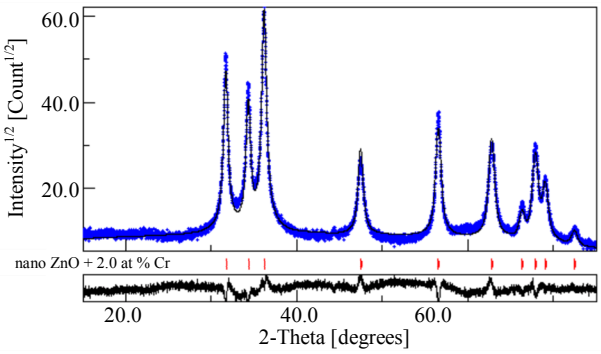

(b)

Figure 4. (a) TEM of 8.0 at% as-prepared powder, and (b) Rietveld XRD refinement showing wurtzite structure.

measured x-ray pattern can be justified using only the wurtzite structural parameters, so there is solid solution even with 8 at% chromium.

Several studies have shown that micrometric ZnO can take Cr_2O_3 in solid solution up to 7 mol%, this solubility limit being modified by the presence of impurities [17]. One of the reasons of this considerable solubility can be justified on the basis of ionic radii values [18] (r_{Cr3+} = 75.5 pm and r_{Zn2+} = 74 pm), hence it is concluded that Cr^{3+} can be incorporated in the cationic sublattice. Nevertheless, when Cr^{3+} is dissolved in the lattice instead of Zn^{2+}, it must be charge compensated by means of a point defect, creating Zn^{2+} vacancies in the bulk, probably by some mechanism like [17]

$$Cr_2O_3 \xrightarrow{(ZnO)} 2Cr_{Zn}^{\bullet} + 3O_O + V_{Zn}'' \qquad (2)$$

Consequently, as Cr^{3+} is incorporated in the lattice, one should expect a small expansion in ZnO lattice parameters because of ionic radii differences.

The presence of Cr-O bonding in ZnO wurtzite structure from synthesized Cr-ZnO solid solutions was determined by energy-dispersive x-ray spectroscopy (**Table 1**) and additionally supported by FTIR spectra as shown in **Figure 5**.

The FTIR spectra of all the ZnO-Cr_2O_3 samples showed the same absorption bands as the ZnO sample (**Figure 1(c)**) together with small absorption bands at 2360 and 2885 cm^{-1}, both corresponding to some O-Cr vibrational modes according to FTIR spectra of Cr_2O_3 (**Figure 2(c)**). When chromium content reaches 16.0 at%, the FTIR spectrum presents the same ZnO absorption bands (1350 to 1800 cm^{-1}) and two more Cr_2O_3 absorp-

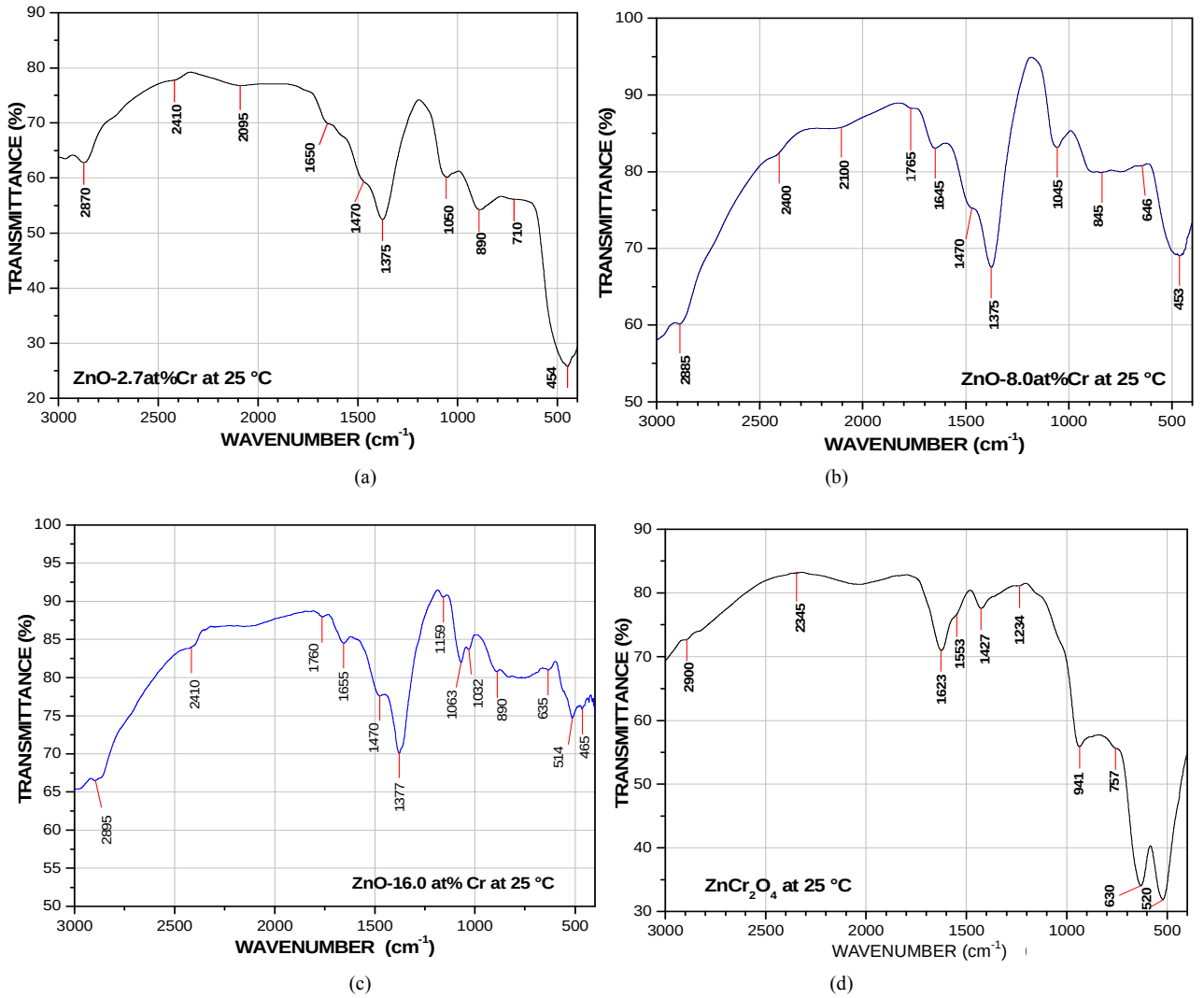

Figure 5. FTIR spectra at room temperature of the nanometric Cr-ZnO particles having different Cr content. (a) 0.65 at%; (b) 8.0 at%; 16.0 at% and (c) 33.3 at%.

tion bands at 514 and 635 cm^{-1}. Finally, at the spinel-composition (**Figure 5(d)**), FTIR spectrum changes considerably due to the enhancement of the Cr_2O_3 absorption bands at 520 and 630 cm^{-1}, remaining the presence of weak absorption bands of ZnO between 1350 and 1800 cm^{-1}.

Figure 6 presents the progression between particle size and lattice parameters ***c*** and ***a*** (of the ZnO hexagonal cell), as a function of the chromium concentration. The results suggest that the hexagonal cell of the nanometric ZnO was, to a certain limit, modified by the Cr^{3+} ions incorporated in the crystal lattice. Therefore, at low chromium content both ***a*** and ***c*** parameters slightly augmented as a consequence of Cr-O bonding inside the ZnO structure. But as the chromium content exceeds of 2.7 at%, there is basically no further expansion of the cell but FTIR spectra indicates that chromium associated to Cr-O bonds exists without the presence of $ZnCr_2O_4$ structure (**Figure 5**). The size effect on structure and lattice parameters has been widely documented and the relative variation of lattice parameter with particle size is given by [19]:

$$\frac{\Delta a}{a} = -\frac{2}{3}\kappa\frac{\gamma}{R} \quad (3)$$

γ and ***R*** are the surface energy and the particle size; κ and ***a*** being the compressibility factor and lattice parameter of the bulk solid respectively.

Therefore, there is a contraction of the crystal lattice due to the pressure exerted toward the interior of the particle. This contraction is proportional to the surface energy and inversely proportional to the particle size, where lattice contraction has been observed experimentally on many solids with particle size reduction [20]. ZnO cell expansion in both ***a*** and ***c*** lattice parameters have been observed on samples prepared by solvothermal synthesis

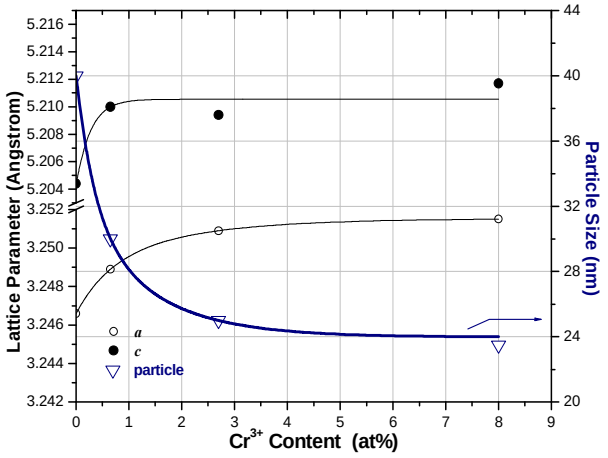

Figure 6. Evolution of particle size and lattice parameters a and c of ZnO as a function of the chromium content.

adding up to 8 mol% chromium [21] and in Cr doped ZnO samples prepared by CVS techniques where no second phases besides wurtzite structure have been observed [7], indicating once again that the chromium ions were incorporated in the ZnO structure. The fact that in this process the incorporation of more than 3 at% Cr^{3+} ions does not modified any longer the ZnO lattice parameters could be associated to the size effect on lattice parameters given by Equation (3). If chromium ions enter in the cationic sublattice but parameters can not change as a consequence of a smaller particle size, then lattice strain must augment in the crystal structure, as shown before in Williamson-Hall plots and the values reported in **Table 1** for parameter η.

4.3. The Thermal Evolution of Zinc-Chromium Oxide Nanoparticles

Even if chemical precipitation using TEA was capable to produce Cr-ZnO solid solution and $ZnCr_2O_4$ spinel as the Cr content increases, almost certainly there will be an inevitable need of heat processing to obtain well crystallized strain-free nanometric zinc-chromium oxides. Of all solid state reactions, the formation of oxide spinels are at present the most systematically investigated compounds [22]. The spinel $ZnCr_2O_4$ is commonly prepared by a solid state reaction of zinc oxide and chromium oxide, where the calcination temperature varies in a range of 800˚C to 1200˚C [23]. In order to assess the influence of thermal treatment on the formation of Cr-ZnO (solid solution) and spinel $ZnCr_2O_4$ nanoparticles, thermal analysis of the different as-prepared compositions was carried out.

We can not expect the same thermal evolution as those reported in the literature by conventional processing [24], for the reason that in this case samples already started with solid solution, quasi-solid solution ($2ZnO{\cdot}Cr_2O_3{\cdot}H_2O$) or spinel composition at room temperature. **Figure** 7 presents the DTA curves plotted for each composition. At low temperature, two endothermic reactions were observed in all samples, the first one being at 122˚C and corresponding to water desorption, the second one at 235˚C corresponding to TEA decomposition; both endothermic peaks being independent of the chromium content. Afterward there was the presence of an exothermic peak at 285˚C probably for all samples, but being notorious for concentrations higher than 2.7 at% chromium. Besides, at high temperature another endothermic process appears at 430˚C, probably as a result of the formation of $ZnCr_2O_4$ from the Cr-ZnO solid. Finally, there was a broad exothermic peak in all thermograms at approximately 550˚C, probably associated to particle growth.

Subsequently, the as-prepared samples were heat treated in oxygen at two different temperatures (400 and

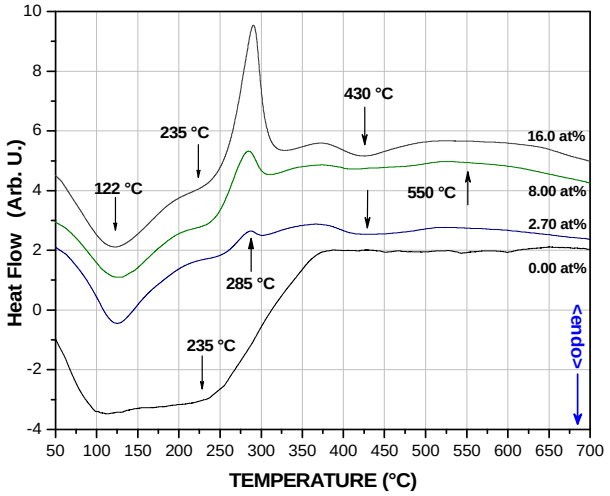

Figure 7. Thermodiagrams of the nanometric Cr-ZnO nanoparticles obtained by DTA using a constant heating rate of 10˚C/min in oxygen.

700˚C), then rapidly cooled and compared by XRD in order to relate the effect of Cr^{3+} during the calcination process observed by DTA. XRD results are shown in **Figure 8**, indicating that phase evolution depends on Cr^{3+} content. Calcinations carried out on samples with 0.65, 2.7 and 8.0 at% at 400˚C (**Figure 8(a)**) lead to the Cr-ZnO solid solution (wurtzite ZnO phase) and it was not possible to distinguish $ZnCr_2O_4$ formation (cubic spinel). On the other hand, in sample with 16 at% chromium, only the Cr-ZnO solid solution was detected by XRD, suggesting the reaction $2ZnO{\cdot}Cr_2O_3 \rightarrow$ Cr-ZnO (solid solution) taking place at 285˚C without formation of $ZnCr_2O_4$. Finally, after annealing of all samples at 700˚C, XRD results showed the presence of $ZnCr_2O_4$ formation from Cr-ZnO solid solution. Probably, the solid state reactions taking place during thermal evolution could be approximated to the following sequence:

$$\begin{aligned} &ZnOCr_2O_3(a) + \text{Cr-ZnO}(s) \\ &\xrightarrow{285^{\circ}C} ZnOCr_2O_3(c) + \text{Cr-ZnO}(s) \\ &\xrightarrow{285^{\circ}C} \text{Cr-ZnO}(ss) \end{aligned} \quad (4)$$

$$\text{Cr-ZnO}(ss) \xrightarrow{285^{\circ}C} \text{Cr-ZnO}(s) + ZnOCr_2O_4(c) \quad (5)$$

where **a:** amorphous, **s:** solid solution, **ss:** Cr^{3+} over concentrated solid solution and **c:** crystalline solid. Therefore, the exothermic peak at 285˚C probably corresponds to both process, crystallization of the $2ZnO{\cdot}Cr_2O_3$ like compound and formation of Cr^{3+} concentrated solid solution, followed of solid solution decomposition to $ZnCr_2O_4$ at 430˚C.

Once again, Williamson-Hall analysis was used to get information about strain distortion and particle size of

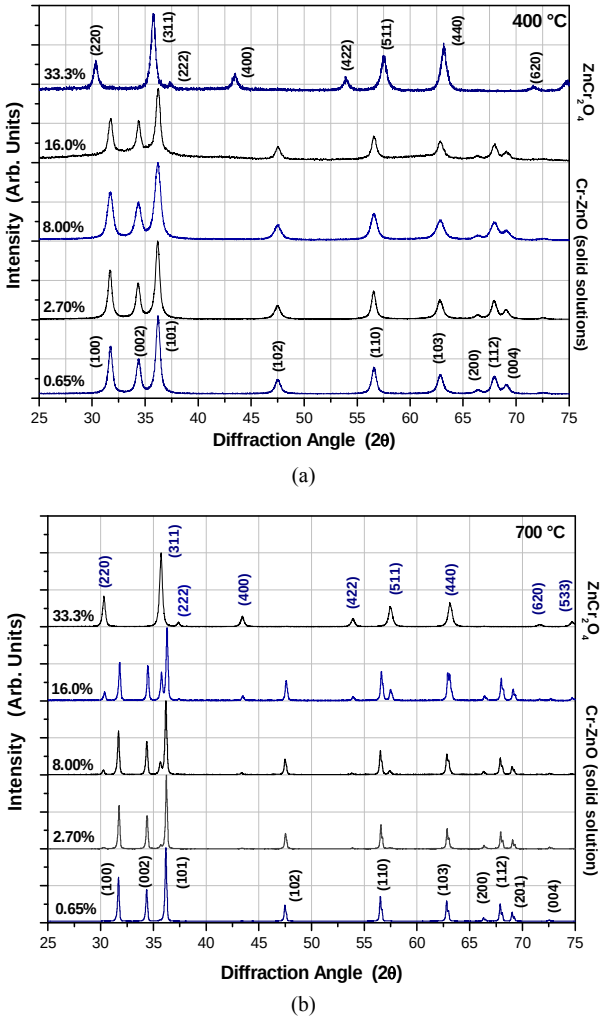

Figure 8. XRD patterns of Cr-ZnO nanoparticles after heat treatment at (a) 400˚C; (b) 700˚C.

ZnO phase in samples as a function of heat treatment and chromium content. **Figures 9(a)** and **9(b)** show the Williamson-Hall plots from XRD data of each sample at 400 and 700˚C. According to the calculated slope η and intersection with vertical axis (λ/**L**) from **Figure 9**, the slope was reduced and particle size was augmented (**Table 2**) as temperature was increased. Nevertheless, in all cases particle size remains in the nanometric domain by means of Cr^{3+} incorporation. TEM bright field images of two different compositions (0.65 and 16.0 at%) at 400 and 700˚C are shown on **Figure 10** to corroborate that Cr-ZnO solid solutions and $ZnCr_2O_4$ particle size remains in the nanometric domain as calculated from Williamson-Hall method.

5. Conclusions

In this work, a technically simple and economical process was used to produce at room temperature nanoparti-

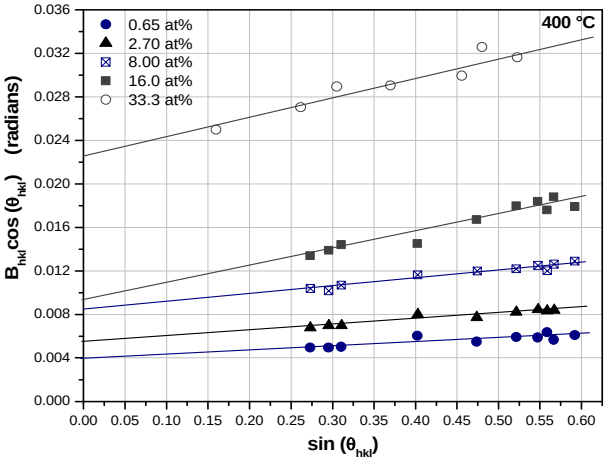

(a)

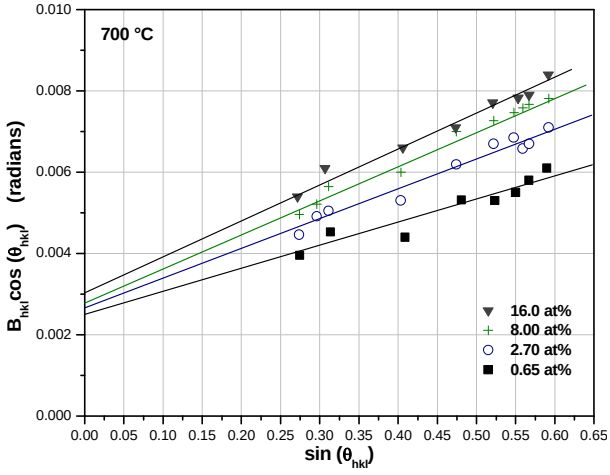

(b)

Figure 9. Williamson-Hall plots of the corresponding XRD patterns of the different Cr-ZnO nanoparticles after heat treatment at (a) 400˚C and (b) 700˚C.

Table 2. Mean particle size and lattice distortion obtained from williamson-hall analysis.

Sample	T = 400˚C		T = 700˚C	
Cr (at%)	**<L> (nm)**	**(%)**	**<L> (nm)**	**(%)**
0.00	57	0.31	95	0.14
0.65	40	0.35	62	0.40
2.70	38	0.54	60	0.76
8.00	29	0.76	55	0.88
16.0	28	0.85	45	0.96
33.3	15	1.85	30*	------

* Estimated from TEM images.

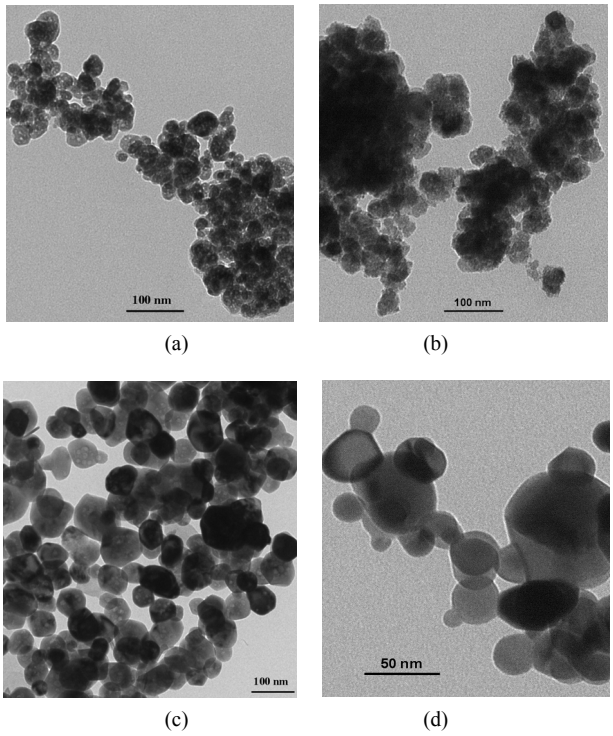

(a) (b)

(c) (d)

Figure 10. (a) and (b) TEM images of 0.65 and 16.0 at% Cr^{3+} after heating at 400˚C. (c) and (d) TEM images of same samples after heating at 700˚C.

cles of single phase Cr-ZnO solid solution and spinel $ZnCr_2O_4$. It was observed that the lattice parameter of the ZnO *a*-axis and ***c***-axis slightly augment as the chromium content increase up to 3 at%. Subsequently, adding more Cr^{3+} into the ZnO structure does not substantially modify the lattice parameters, probably as a consequence of cell contraction effect from particle size reduction according to Equation (3). Nevertheless, EDS and IR spectra indicated that chromium atoms are incorporated during the TEA aqueous precipitation in the wurtzite Cr-ZnO solid solution up to 8 at% and do not forms a second phase in the range of room temperature up to 400˚C. Besides, it was observed at room temperature using a higher chromium content (16.0 at%), the presence of a second compound, probably of the form $2ZnO{\cdot}Cr_2O_3{\cdot}nH_2O$, transforming at 400˚C into a Cr-ZnO solid solution incorporating 16.0 at% chromium in the wurtzite ZnO structure and remaining in the nanometric domain (30 nm). The most plausible solid state reactions involved during thermal treatment were proposed according to reactions (4) and (5). Finally, crystalline strain-free $ZnCr_2O_4$ nanoparticles can be promoted with annealing treatment at 400˚C.

REFERENCES

[1] T. Brock, M. Groteklaes and P. Mischke, "European

Coatings Handbook," Vincentz Verlag, Hannover, 2000.

[2] J. Uhm, M. Shin, Z. Jiang and J. Chung, "Selective Oxidation of H_2S to Elemental Sulfur over Chromium Oxide Catalysts," *Applied Catalysis B*: *Environment*, Vol. 22, No. 4, 1999, pp. 293-303. doi:10.1016/S0926-3373(99)00057-0

[3] M. Bkjker, J. Bastiaens, E. Draaisma, L. de Jong, E. Sourty, S. Saied and J. Sullivan, "The Development of a Thin Cr_2O_3 Wear Protective Coating for the Advanced Digital Recording System," *Tribology International*, Vol. 32, No. 4-6, 2003, pp. 227-233. doi:10.1016/S0301-679X(02)00191-3

[4] Y. Shimizu, S. Kusano, *et al*., "Oxigen Sensing Properties of Spinel-Type Oxides for Stoichiometric Air/Fuel Combustion Control," *Journal of the American Ceramic Society*, Vol. 73, No. 4, 1990, pp. 818-824. doi:10.1111/j.1151-2916.1990.tb05120.x

[5] M. Shinoda, T. Nishide, Y. Sawada, M. Hosaka and T. Matsumoto, "Stability of Sputter Deposited ZnO:Cr Films Against Acids," *Japanese Journal of Applied Physics*, Vol. 32, Part 2, No.10B, 1993, pp. L1565-L1567.

[6] V. Sharma, *et al*., "Synthesis and Characterization of Nanocrystalline $Zn_{1-x}MO$ (M = Ni, Cr) Thin Films for Efficient Photoelectrochemical Splitting of Water," *International Journal of Hydrogen Energy*, Vol. 36, 2011, pp. 4280-4290. doi:10.1016/j.ijhydene.2011.01.004

[7] W. Jin, I. Lee, A. Kompch, U. Dorfler and M. Winterer, "Chemical Vapor Synthesis and Characterization of Chromium Doped Zinc Oxide Nanoparticles," *Journal of the European Ceramic Society*, Vol. 27, No.13-15, 2007, pp. 4333-4337. doi:10.1016/j.jeurceramsoc.2007.02.152

[8] Z. Marinkovic, L. Mancic, P. Vulic and O. Milosevic, "Microstructural Characterization of Mechanically Activated ZnO-Cr_2O_3 System," *Journal of the European Ceramic Society*, Vol. 25, No. 12, 2005, pp. 2081-2084. doi:10.1016/j.jeurceramsoc.2005.03.085

[9] J. Merchant and M. Cociver, "Preparation and Doping of Zinc Oxide Using Spray Pyrolysis," *Chemistry of Materials*, Vol. 7, No. 9, 1995, pp. 1742-1749. doi:10.1021/cm00057a026

[10] A. Ennaqadi, M. Khaldi, A. Roy, C. Forano and J. Besse, "XFAS Study of Structural Evolution during Calcination of Two Zinc-Chromium Based Lamellar Double Hydroxides," *Journal de Physique* 4, Vol. 7, No. C2, 1997, pp. 1231-1232.

[11] A. Sen and P. Pramanik, "Preparation of Nano-Sized Calcium, Magnesium and Zinc Chromite Powders through Metallo-Organic Precursor Solutions," *Journal of Material Synthesis and Processing*, Vol. 10, No. 3, 2002, pp 107-111. doi:10.1023/A:1021980211341

[12] Q. Zhongl and E. Matijevik, "Preparation of Uniform Zinc Oxide Colloids by Controlled Double-Jet Precipitation," *Journal of Material Chemistry*, Vol. 6, No. 3, 1996, pp. 443-448. doi:10.1039/jm9960600443

[13] M. Andres-Verges and C. J. Serna, "Morphological Characterization of ZnO Powders by x-ray and IR Spectroscopy," *Journal of Materials Science*, Vol. 7, No.4, 1998, pp. 970-972.

[14] T. Ivanova, *et al*., "Structural Transformations and their Relation to the Optoelectronic Properties of Chromium Oxide Thin Films," *Journal of Physics*: *Conference Series*, Vol. 13, 2008, pp. 12030-12034. doi:10.1088/1742-6596/113/1/012030

[15] J. Matthies, L. Lutterotti and H. Wenk, "Advances in Texture Analysis from Diffraction Spectra," *Journal of Applied Crystalography*, Vol. 30, No. 1, 1997, pp. 31-42. doi:10.1107/S0021889896006851

[16] G. K. Williamson and W. H. Hall, "X-ray Line Broadening from Filed Aluminum and Wolfram," *Acta Metallurgica*, Vol. 1, No. 1, 1953, pp. 22-31. doi:10.1016/0001-6160(53)90006-6

[17] A. M. Gadalla, "Compatible Phases in the System Zinc Oxide-Copper (II) Oxide-Copper-Chromium (III) Oxide," *Industrial Engineering and Chemistry Fundamentals*, Vol. 23, No. 4, 1984, pp. 436-440. doi:10.1021/i100016a010

[18] C. Giacovazzo, "Fundamentals of Crystallography," Oxford University Press, Oxford, 2000.

[19] C. Henry, "Size Effects on Structure and Morphology of Free or Supported Nanoparticles," in: C. Brechignac, P. Houdy and M. Lahmani, Eds., *Nanomaterials and Nanochemistry*, Springer-Verlag, Berlin, 2007, pp. 1-34.

[20] J. Woltersdorf, A. S. Nepijko and E. Pippel, "Dependence of Lattice Parameters of Small Particles on the Size of the Nuclei," *Surface Science*, Vol. 106, No. 1-3, 1981, pp. 64-69. doi:10.1016/0039-6028(81)90182-5

[21] W. Lojkowski, *et al*., "Solvothermal Synthesis of Nanocry-Stalline Zinc Oxide Doped with Mn^{2+}, Ni^{2+}, Co^{2+} and Cr^{3+} Ions," *Journal of Nanoparticle Research*, Vol. 11, No. 8, 2009, pp. 1991-2002. doi:10.1007/s11051-008-9559-9

[22] H. Schmalzried, "Chemical Kinetics of Solids," VCH, Berlin, 1995. doi:10.1002/9783527615537

[23] T. Ishii, R. Furuichi and Y. Hara, "Thermoanalytical Study of the Solid State Reactions in MgO-Cr_2O_3 and ZnO-Cr_2O_3 Systems," *Journal of Thermal Analysis and Calorimetry*, Vol. 11, No. 1, 1977, pp. 71-80. doi:10.1007/BF02104085

[24] T. Konvicka, P. Mosner and Z. Solc, "Investigation of the Non-Isothermal Kinetics of the Formation of $ZnFe_2O_4$ and $ZnCr_2O_4$," *Thermal Analysis and Calorimetry*, Vol. 60, No. 2, 2000, pp. 629-640. doi:10.1023/A:1010115625642

